http://dx.doi.org/10.5012/bkcs.2014.35.6.1647

Synthesis and Characterization of Phenanthrene-substituted Fullerene Derivatives as Electron Acceptors for P3HT-based Polymer Solar Cells

Dongbo Mi, Jong Baek Park, Fei Xu, Hee Un Kim, Ji-Hoon Kim, and Do-Hoon Hwang*

Department of Chemistry, and Chemistry Institute for Functional Materials, Pusan National University, Busan 609-735, Korea
**E-mail: dohoonhwang@pusan.ac.kr*
Received December 3, 2013, Accepted February 6, 2014

9,10-Bis(bromomethyl)phenanthrene reacted with fullerenes *via* a Diels-Alder reaction to give phenanthrene-substituted fullerene mono-adducts (PCMA) and bis-adducts (PCBA) as electron acceptors for organic photovoltaic cells (OPVs). The syntheses of the fullerene derivatives were confirmed by ^{1}H ^{13}C NMR spectroscopy and MALDI-TOF mass spectrometry. PCMA and PCBA showed better light absorption in the UV-visible region than $PC_{61}BM$. Their electrochemical properties were measured using cyclic voltammetry. Accordingly, the lowest unoccupied molecular orbital (LUMO) energy levels of PCMA and PCBA were −3.66 and −3.57 eV, respectively. Photovoltaic cells were fabricated with a ITO/PEDOT:PSS/poly(3-hexylthiophene)(P3HT):acceptor/LiF/Al configuration, where P3HT and PCBA are the electron donors and acceptors, respectively. The polymer solar cell fabricated using the P3HT:PCBA active layer showed a maximum power conversion efficiency of 0.71%.

Key Words : Phenanthrene-substituted fullerene, Electron acceptor, Organic photovoltaic cells

Introduction

Solar cells are important technology for the production of renewable energy.[1] Despite the expanding use of inorganic semiconductors in photovoltaic cells, organic semiconductors are very promising as they enable the relatively inexpensive fabrication of lightweight, flexible solar modules that can be used in large-area devices.[2-11] The exploration of new organic semiconducting materials with novel electronic properties has become an exciting research area. The electrical properties of these materials are of both academic and industrial interest. Recently, the power conversion efficiencies (PCEs) of organic photovoltaic cells (OPVs) have undergone a rapid improvement due to the development of new polymeric or molecular donor materials and have reached maximum values of ~7–9%[12-15] using conventional or inverted device structures. In addition to acting as donor materials, fullerene derivative acceptors could also be used to boost power conversion efficiency by controlling the energy levels of their frontier orbitals.[16-21] In particular, fullerene *bis*-adducts have attracted significant attention with respect to increasing the open circuit voltage (V_{oc}) of OPVs because they have a high lowest unoccupied molecular orbital (LUMO) energy level. For example, the LUMO energy level of *bis*[6,6]-phenyl-C_{61}-butyric acid methyl ester (*bis*-PCBM) is ~0.1 eV higher than that of the $PC_{61}BM$ mono adduct. Accordingly, the OPV fabricated using P3HT/*bis*-$PC_{61}BM$ showed a higher V_{oc} (0.73 V) than the device fabricated using P3HT/$PC_{61}BM$ (~0.60 V).[22] The LUMO energy level of indene-C_{60} *bis*-adduct ($IC_{60}BA$) is 0.17 eV higher than that of $PC_{61}BM$; [23] therefore, the device fabricated using P3HT:$IC_{60}BA$ has a very high V_{oc} (0.84 V).

Herein, we design and synthesize phenanthrene-substituted fullerene mono-adducts (PCMA) and bis-adducts (PCBA) *via* a Diels-Alder reaction as electron acceptors for OPVs. We expect that the synthesized fullerenes will have enhanced light-harvesting ability because the aromatic phenanthrene groups are larger than those in $PC_{61}BM$. Furthermore, the *bis*-adducts could show a high LUMO energy level. The synthetic routes and chemical structures of PCMA and PCBA are shown in Scheme 1.

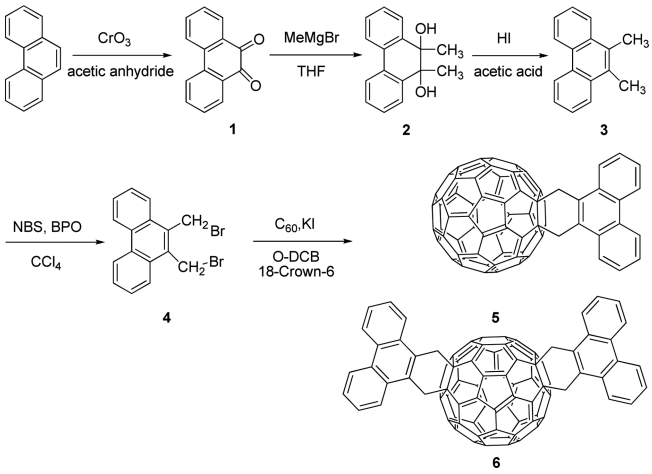

Scheme 1. Synthetic routes and chemical structures of PCMA and PCBA.

Experimental

Materials. Phenanthrene, chromium(VI) oxide, acetic anhydride, 2-propanol, methyl magnesium chloride, acetic acid, hydroiodic acid, sodium bisulfate, benzoyl peroxide, carbon disulfide, fullerene (C60), potassium iodide, 18-crown-6,

1,2-dichlorobenzene, and *N*-bromosuccinimide were purchased from Aldrich. All chemicals and solvents (analytical grade) were used without further purification.

Measurements and Device Fabrication. ^{1}H and ^{13}C NMR spectra were recorded using a Varian AM-300 spectrometer. UV-Visible absorption spectra were recorded using a Scinco S-3100 spectrometer, elemental analysis (EA) was performed using a vario MICRO cube spectrometer, and MALDI-TOF mass spectra were measured using a Voyager-DE STR. Cyclic voltammetry (BAS 100) was performed at a scan rate of 50 mV/s using a tetrabutylammonium tetrafluoroborate ($TBABF_4$, 0.10 M in anhydrous 1,2-dichlorobenzene) solution as the electrolyte and a 1,2-dichlorobenzene solution of the sample (10^{-3} M) at room temperature under an argon atmosphere. A glassy carbon electrode (0.3 mm diameter) was used as the working electrode, and Pt and Ag/AgCl electrodes were used as the counter and reference electrodes, respectively. A composite solution of P3HT and PCBA was prepared in 1,2-dichlorobenzene. The concentration of the composite solution was maintained at 15 mg/mL. OPVs with a structure of ITO/PEDOT:PSS/P3HT:PCBA/LiF/Al were fabricated. The ITO-coated glass substrates were cleaned by consecutive sonication in a detergent, distilled water, acetone, and, finally, 2-propanol. After exposing the ITO surface to ozone for 20 min, PEDOT:PSS (Clevios P) was spin-coated onto the ITO substrate. The PEDOT:PSS layer was dried on a hot plate at 150 °C for 15 min. The pre-dissolved composite solution was filtered through 0.2 μm syringe filters then spin-coated onto the PEDOT:PSS layer to form the active layer. Finally, a cathode (top electrode) consisting of LiF and Al was deposited onto the active layer in a thermal evaporator under a vacuum of 3×10^{-6} Torr. The current–voltage (I–V) characteristics of all the OPVs were measured under simulated solar light (100 mW/cm^2; AM 1.5 G) provided by a K201 Lab50 solar simulator (McScience Inc.). Electrical data were recorded using a K101 Lab 20 photovoltaic power meter (McScience Inc.) source-measure unit, and all characterizations were carried out in the ambient environment. The intensity of the simulated sunlight was calibrated using a standard Si photodiode detector (K801S-K11; McScience Inc.). Measurements were performed after masking all but the active cell area of the fabricated device, which was 9 mm^2. All the characterization steps were performed under ambient laboratory air.

Synthesis of Phenanthrene-9,10-dione (1). Phenanthrene (5.0 g, 0.028 mol) was added to a 1 L flask and dissolved in 300 mL of acetic anhydride. Chromium(VI) oxide (6.16 g, 0.062 mol) was slowly added to the flask, which was in an ice bath. After 3 h of reaction, the excess ice was poured into the reaction mixture. Yellow crude product was obtained after filtration and washed with distilled water until the effluent liquid was colorless. Yellow crystals were obtained after recrystallization of the crude product from a toluene/ethanol (v/v = 3:1) co-solvent. The yield was 50.39% (2.94 g). ^{1}H NMR (300 MHz, $CDCl_3$) δ 8.20 (dd, 2H), 8.03 (d, 2H), 7.74 (dt, 2H), 7.5 (dt, 2H).

Synthesis of 9,10-Dimethyl-9,10-dihydrophenanthrene-9,10-diol (2). A solution of compound **1** (2 g, 9.61 mmol) in 120 mL of THF was added into a 250 mL one-necked flask. A methylmagnesium chloride solution in THF (3 M; 8.34 mL, 24.01 mmol) was added drop-wise into the flask for 10 min. The reaction mixture was stirred for 2 h and then quenched with 0.25 M aqueous HCl. The reaction mixture was thrice extracted with acetic ether. The combined extracts were dried with anhydrous magnesium sulfate and concentrated using a rotary evaporator. The crude product was purified by column chromatography using ethyl acetate/hexane (v/v = 1:4) as the eluent. The yield of the resulting white solid (**2**) was 77.02% (1.78 g). ^{1}H NMR (300 MHz, acetone-d_6) δ 7.80 (m, 4H), 7.38 (m, 4H), 3.65 (s, 2H), 1.35 (s, 6H).

Synthesis of 9,10-Dimethylphenanthrene (3). A solution of compound **2** (1.5 g, 6.24 mmol) in 50 mL of acetic acid was added into a 100 mL two-necked flask followed by the slow addition of 2.13 mL of 57% aqueous HI. The solution was refluxed overnight. After cooling to room temperature, the reaction mixture was poured into 1% aqueous sodium bisulfate solution. The resultant precipitate was collected by filtration and further purified through column chromatography using toluene/hexane (v/v = 1:9) as the eluent. The yield of the resulting yellow solid (**3**) was 87.4% (1.13 g). ^{1}H NMR (300 MHz, $CDCl_3$): δ 8.78 (dd, 2H), 8.20 (dd, 2H), 7.70 (m, 4H), 2.78 (s, 6H).

Synthesis of 9,10-Bis(bromomethyl) phenanthrene (4). Compound **3** (1.0 g, 4.85 mmol) was dissolved in 20 mL of carbon tetrachloride. Then, benzoyl peroxide (1.90 g, 10.67 mmol) was slowly added to the reaction mixture and the mixture was refluxed for 24 h. After cooling to room temperature, the reaction mixture was extracted using dichloromethane and brine. The organic layer was dried with anhydrous magnesium sulfate and concentrated in a rotary evaporator. The crude product was further purified by column chromatography using ethyl acetate/hexane (v/v = 1:9) as the eluent and then recrystallized from a dichloromethane (MC) and methanol co-solvent. The yield of the resulting yellow crystals (**4**) was 50% (0.88 g). ^{1}H NMR (300 MHz, $CDCl_3$) δ 8.80 (dd, 2H), 8.21 (dd, 2H), 8.70 (m, 4H), 5.10 (s, 4H).

Synthesis of PCMA (5). A mixture of C_{60} (0.3 g, 0.42 mmol), compound **4** (0.182 g, 0.5 mmol), potassium iodide (0.33 g, 2.0 mmol), and 18-crown-6 (0.53 g, 2.0 mmol) was dissolved in anhydrous 1,2-dichlorobenzene, and the reaction mixture was refluxed for 48 h under an Ar atmosphere in the dark. After cooling to room temperature, the reaction mixture was adsorbed on silica gel and purified by flash silica column chromatography (Merck silica gel 60, 230–400 mesh) with a hexane/toluene (v/v = 5:1) mixture as the eluent. The desired product was concentrated *in vacuo* and precipitated in excess MeOH to give a brown solid. The product yield was 59 mg (15.4%). ^{1}H NMR (300 MHz, $CDCl_3/CS_2$) δ 8.95 (m, 2H), 8.52 (m, 2H), 7.78 (m, 4H), 5.10 (bs, 4H). ^{13}C NMR (75 MHz, $CDCl_3/CS_2$) δ 156.25, 146.45, 146.20, 145.41, 144.66, 143.05, 142.57, 142.21, 142.05, 133.23, 130.02, 128.25. Elemental analysis for $C_{76}H_{12}$: calculated: C, 98.69; H, 1.31; found: C, 96.21; H, 1.29 (purity: 97.49%). MALDI-TOF MS:

calculated for $C_{76}H_{12}$, 924.91; found: 924.29 (M^+).

Synthesis of PCBA (6). The synthesis of PCBA is similar to that of PCMA (**5**). Fullerene (0.3 g, 0.42 mmol) was reacted with compound **4** (0.333 g, 0.92 mmol), potassium iodide (0.61 g, 3.66 mmol), and 18-crown-6 (0.97 g, 3.66 mmol). PCBA was purified *via* silica column chromatography with hexane/toluene (v/v = 1:1) as the eluent. The product yield was 127 mg (27.1%). ^{1}H NMR (400 MHz, $CDCl_3/CS_2$) δ 8.90–8.80 (m, 4H), 8.70–8.20 (m, 4H), 7.70–7.40 (m, 8H), 5.40–4.40 (bm, 8H). ^{13}C NMR (75 MHz, $CDCl_3/CS_2$) δ 30.01, 65.32, 123.74, 126.65, 126.74, 127.53, 127.80, 129.19, 130.28, 130.68, 133.28, 141.47, 141.88, 143.25, 144.08, 144.87, 145.65, 146.41, 146.66, 148.74, 154.30. Elemental analysis for $C_{92}H_{24}$: calculated: C, 97.86; H, 2.14; found: C, 96.21; H, 2.10 (purity: 98.31%). MALDI-TOF MS: calculated for $C_{92}H_{24}$, 1129.17; found: 1129.22 (M^+).

Results and Discussion

Identification of PCMA and PCBA. PCMA and PCBA fullerene derivatives were synthesized though a [4+2] cycloaddition between fullerene and the diene intermediate generated from 9,10-bis(bromomethyl) phenanthrene (compound **4**). It is known that fullerenes can be functionalized through this method using exactly 1.0 and 2.0 equivalents of compound **4** to produce PCMA and PCBA as the major products, respectively.[24]

The molecular weights of the two fullerene derivatives were identified by MALDI-TOF mass spectrometry. The spectra of PCMA and PCBA showed molecular ion peaks corresponding to the *mono*- and *bis*-adducts, respectively, as shown in Figure 1.

The ^{1}H NMR spectrum clearly shows characteristic peaks for PCMA (Figure 2(a)). As is evident in the ^{1}H NMR spectra of many fullerene derivatives, the protons of the carbons attached to fullerene are influenced by the anisotropic deshielding field effect of the C_{60} core and thus appear downfield. The characteristic low-field aromatic proton (H_b) and methylene proton (H_a) peaks appear at 8.95, as a doublet, and 5.10 ppm, as a broad singlet, respectively, which strongly supports the formation of an adduct between fullerene and phenanthrene. The peaks corresponding to the other protons on the phenanthrene ring (*i.e.*, H_c, H_d, and H_e) are less downfield shifted than those of H_a and H_b because

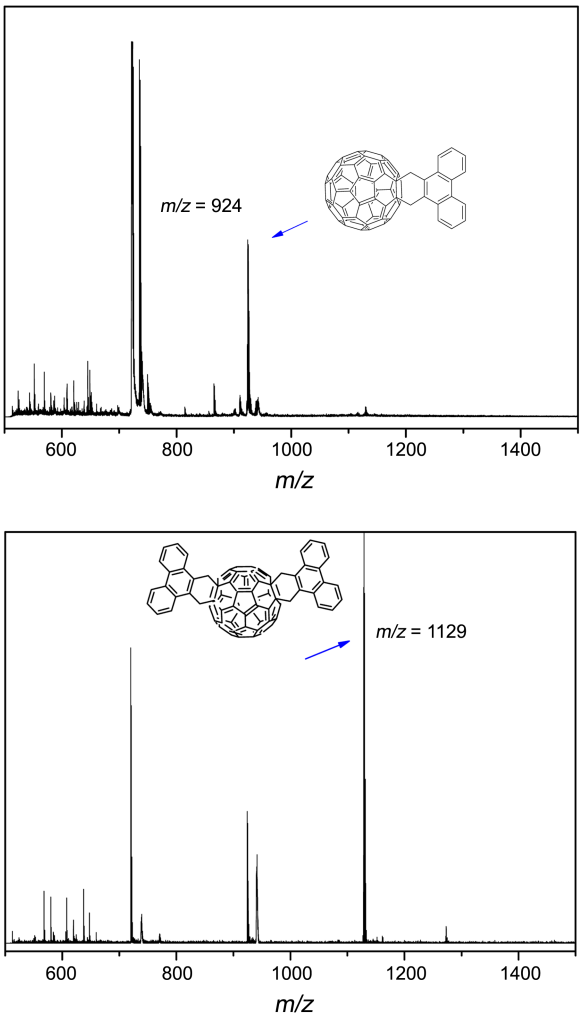

Figure 1. MALDI-TOF mass spectra of PCMA (above) and PCBA (below).

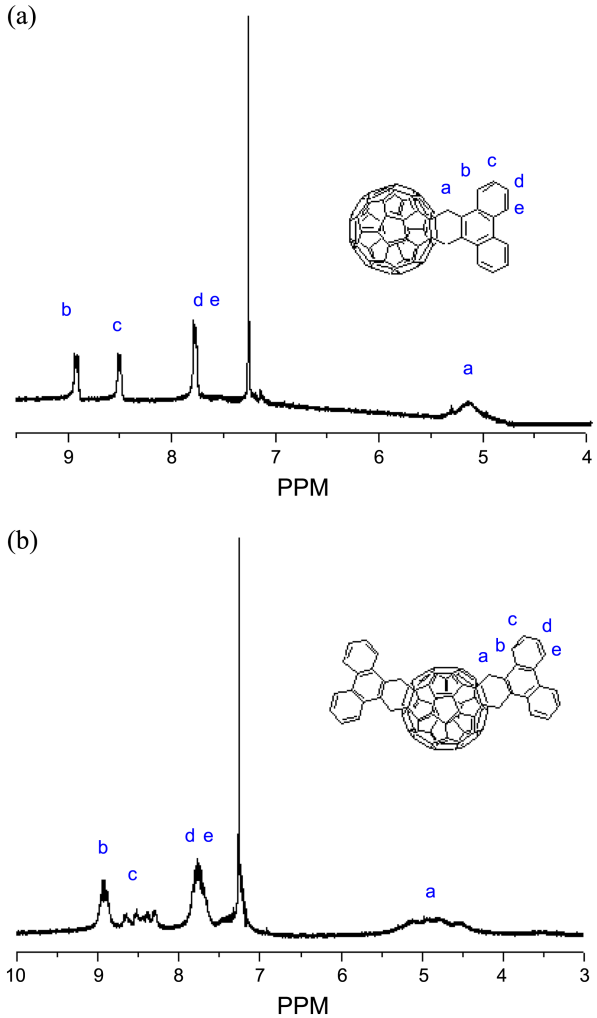

Figure 2. (a) ^{1}H NMR ($CDCl_3$, 300 MHz) spectrum of PCMA. (b) ^{1}H NMR ($CDCl_3/CS_2$, 300 MHz) spectrum of PCBA.

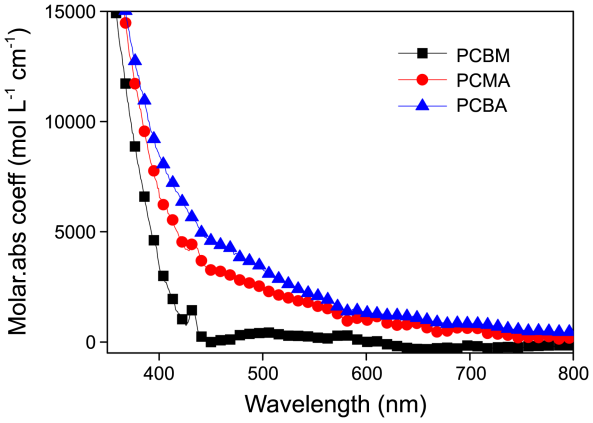

Figure 3. UV-Visible absorption spectra of $PC_{61}BM$, PCMA, and PCBA (in 1,2-dichlorobenzene, 10^{-5} M).

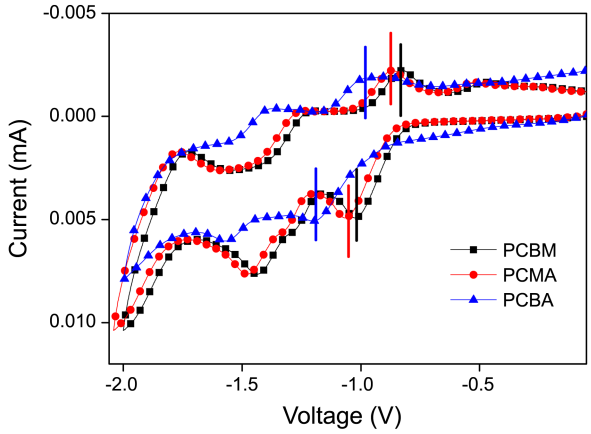

Figure 4. Cyclic voltammograms of $PC_{61}BM$, PCMA, and PCBA.

they are more separated from the fullerene. In the ^{1}H NMR spectrum of PCBA, the peaks in the aromatic regions and the methylene peak are in a similar region as in the spectrum of PCMA, but are broader and more complex. The ^{1}H NMR spectrum of PCBA is shown in Figure 2(b).

Solubility and Optical Properties. PCMA and PCBA showed moderate solubility in 1,2-dichlorobenzene, but limited solubility in other common organic solvents, such as chloroform and toluene. PCBA showed better solubility than PCMA. The UV-visible absorption spectra of $PC_{61}BM$, PCMA, and PCBA in 1,2-dichlorobenzene (10^{-5} M) are shown in Figure 3. It is evident that PCMA and PCBA have higher molar absorption coefficients than $PC_{61}BM$ throughout the spectral range (300–600 nm). PCBA had the highest molar absorption coefficient, as shown in Figure 3. The spectrum of PCMA exhibited a small, but sharp, absorption peak at 432 nm similar to that of $PC_{61}BM$. However, the spectrum of PCBA does not feature any sharp absorption peaks, which is possibly due to the presence of several positional isomers.

Electrochemical Properties of PCMA and PCBA. The LUMO energy level of the acceptor is very important in OPVs because the energy gap between it and the HOMO energy level of the donor polymer is proportional to the V_{oc}. The electrochemical properties of PCMA and PCBA were studied *via* cyclic voltammetry using 1,2-dichlorobenzene and $TBABF_4$ as the solvent and electrolyte, respectively.

The fullerene derivatives exhibit several quasi-reversible one-electron reduction waves, as shown in Figure 4; these are attributed to the fullerene core. The first reduction potential (E^1_{red}) corresponds to the LUMO energy level of the fullerene derivatives. The first reduction potentials of both PCMA and PCBA are in a more negative region than that of $PC_{61}BM$, which indicates that the LUMO energy levels of PCMA and PCBA are higher than that of $PC_{61}BM$. The measured electrochemical properties are summarized in Table 1. The LUMO energy level was calculated from the onset reduction potential (E_{Red}(onset)) with respect to the reference energy level of ferrocene (4.8 eV below vacuum level; vacuum level is defined as zero), as follows:[25] LUMO = $-[(E_{Red}(onset) - E_{foc}) + 4.8]$ (eV), where E_{foc} is the potential of the external standard, *i.e.*, the ferrocene/ferrocenium ion (Foc/Foc+) couple. The value of E_{foc} determined under the same conditions is ~265 mV *vs.* Ag/AgCl. The values of E_{Red}(onset) for PCMA and PCBA are −0.88 and −0.97 V, respectively. Thus, the LUMO energy levels of PCMA and PCBA relative to the vacuum level were estimated to be −3.66 and −3.57 eV, respectively. The introduction of substituents to fullerene breaks its highly uniform spherical conjugated system; thus, the LUMO energy levels of substituted fullerenes are usually higher than that of fullerene. Accordingly, fullerene *bis*-adducts generally have higher LUMO energy levels than that of the corresponding *mono*-adduct.

Table 1. Cyclic voltammetric properties of $PC_{61}BM$, PCMA, and PCBA

	E^1_{red} (V)	E^2_{red} (V)	E^{red}_{onset} (V)	LUMO (eV)
$PC_{61}BM$	−1.01	−1.40	−0.84	−3.70
PCMA	−1.05	−1.44	−0.88	−3.66
PCBA	−1.19	−1.57	−0.97	−3.57

Photovoltaic Performance. Because of the limited solubility of PCMA in organic solvents, macroscopic nanoparticles were found in the blending active layer after spin-coating. The fabricated OPVs showed very high series resistance and no detectable photovoltaic effect due to the poor state of the film. Fortunately, PCBA showed better film characteristics than PCMA after blending with P3HT. The photovoltaic performances of P3HT/PCBA bulk heterojunction devices were investigated using a device structure of ITO/PEDOT:PSS/P3HT-PCBA (1:0.7)/LiF/Al. In order to optimize the device fabrication procedure, the fabricated devices were annealed at 100, 120, and 150 °C for 15 min. The fabricated devices were analyzed under AM 1.5G illumination with a light intensity of 100 mW/cm^2.

The I–V curves of the devices are shown in Figure 5. The power conversion efficiencies (PCEs) of the PCBA-based OPV cells were improved by thermal annealing. This im-

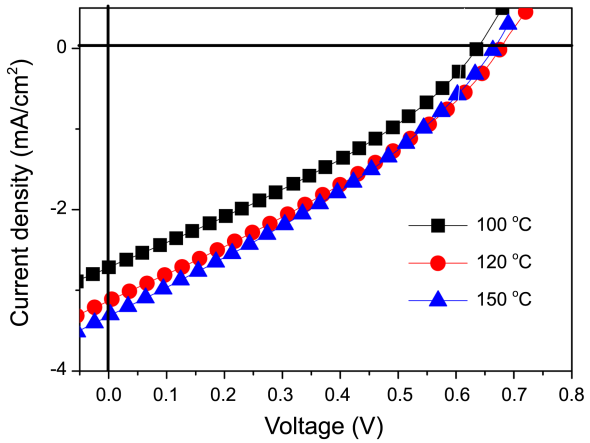

Figure 5. Current–voltage (I–V) curves of the devices (P3HT/PCBA = 1:0.7).

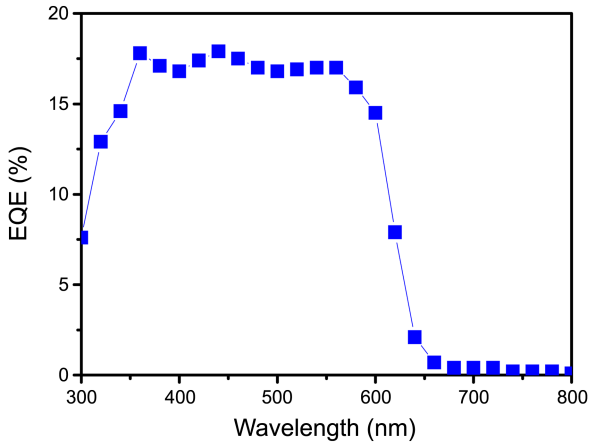

Figure 6. External quantum efficiencies (EQEs) curve of P3HT/PCBA (1:0.7) annealed at 150 °C for 15 min.

provement could be attributed to enhanced J_{sc} values indicating that the mobility of the charge carriers in the active layer was improved by thermal treatment. The maximum V_{oc} of the device fabricated using PCBA:P3HT was 0.68 V, which is 70 mV higher than that of a $PC_{61}BM$:P3HT device. This increase is attributed to the higher LUMO energy level of PCBA than that of $PC_{61}BM$. The maximum PCE from the device fabricated using a P3HT/PCBA (1:0.7) active layer after thermal annealing at 150 °C for 15 min is 0.71% with a V_{oc} of 0.67 V, J_{sc} of 3.31 mA/cm^2, and fill factor (*FF*) of 0.32. Even though the solubility of PCBA is better than that of PCMA, it was insufficient for the preparation of a smooth and high-quality active-layer film with P3HT using a processing solvent such as 1,2-dichlorobenzene. Thus, the poor film quality of the active layer is the main reason for the low J_{sc} and *FF* values of the fabricated devices. Figure 6 presents the external quantum efficiencies (EQEs) of the OPV device fabricated under the optimized conditions: The maximum EQE, which was obtained at 440 nm, was 17.90%. The photovoltaic performances of the fabricated devices are summarized in Table 2.

Electron Mobility. Charge carrier mobility is one of the major concerns in designing organic photovoltaic materials. The electron mobility of PCBA was investigated by the space-charge-limited current (SCLC) method[26] with a device structure of ITO/ZnO (25 nm)/P3HT-PCBA (1:0.7, 110 nm)/LiF (0.5 nm)/Al. For the electron-only devices, SCLC is described by:

Table 2. Photovoltaic properties of P3HT/PCBA (1:0.7) derivatives based on BHJ OPVs

	Annealing	V_{oc} (V)	J_{sc} (mA/cm^2)	FF (%)	PCE (%)
P3HT/PCBA(1:0.7)	100 °C	0.64	2.72	31.95	0.55
P3HT/PCBA(1:0.7)	120 °C	0.68	3.13	31.90	0.68
P3HT/PCBA(1:0.7)	150 °C	0.67	3.31	32.02	0.71
P3HT/$PC_{61}BM$(1:0.7)	150 °C	0.61	9.60	56.14	3.29

$$J = (8/9)\,\varepsilon_r\,\varepsilon_0\,\mu_e\,(V^2/L^3)$$

Where J is the current density, ε_r is the dielectric constant of PCBA, ε_0 is the permittivity of vacuum, L is the thickness of the blend film, and μ_e is the electron mobility. Figure 7 shows the J-V characteristics of the electron-only P3HT/PCBA blend films. The values of electron mobility were calculated from the plots of ln (J) versus ln (V). The electron mobility of PCBA was evaluated to be 2.4×10^{-10} cm^2 V^{-1} S^{-1} at pristine state and increased to 3.2×10^{-10} cm^2 V^{-1} S^{-1} after thermal annealing process at 150 °C for 15min. The electron mobility values of PCBA are much lower than that of $PC_{61}BM$ (2.0×10^{-3} cm^2 V^{-1} S^{-1})[27] possible due to the poor film quality of the active layer. The increase of the electron mobility of the thermally annealed P3HT/PCBA blending film is consistent with the increased J_{sc} after the thermal annealing.

Morphology. The morphology of the photoactive layer is important in OPVs. The morphology of P3HT/PCBA (1:0.7, w/w) blending film was investigated using an atomic force microscopy (AFM). The height, phase, and 3D images (2 μm × 2 μm) of the active layer are shown in Figure 8. In the AFM height images, the bright chain-like bumps would correspond to P3HT segments, and the dark valleys to PCBA segments, similarly, the red colored regions in the phase images (insert images) would correspond to P3HT domains and the blue colored regions to PCBA domains. The pristine film showed root mean square (RMS) around 3.82 nm and the RMS was slightly reduced to 3.14 nm after thermal annealing at 150 °C for 15 min. It should be noted that the higher RMS values at pristine state are attributed to the poor solubility of PCBA and its inefficient miscibility with P3HT since the height of P3HT segments were fluctuated significantly with some segments higher than 40 nm and other segments less than 20 nm as shown in 3D images. In this case, the morphology was not suitable for charge transportation, which could be one possible reason for lower J_{sc} and PCE values at pristine state. Improved self-organization of crystalline P3HT could be obviously found after thermal

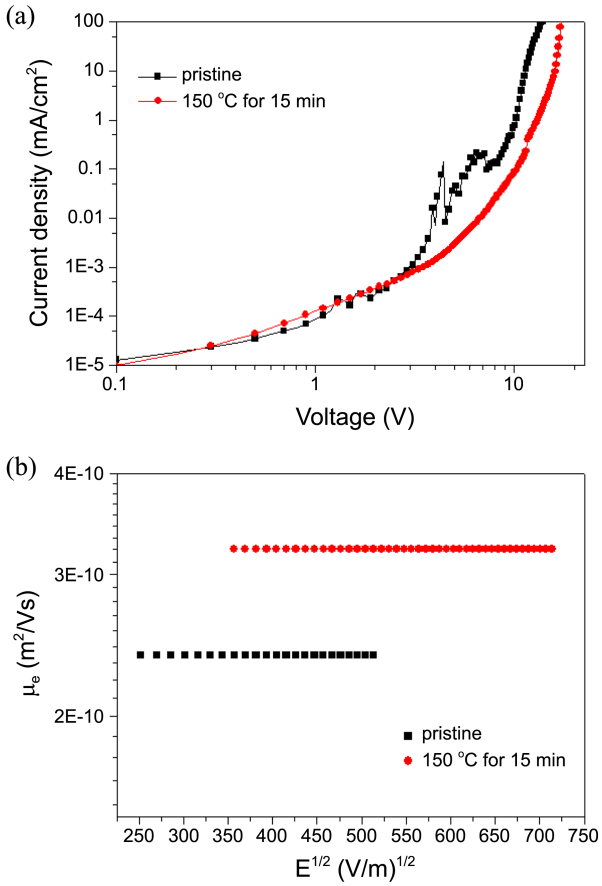

Figure 7. (a) J-V characteristics of the electron-only device of P3HT/ PCBA blend film (1:0.7, w/w). (b) Electron mobility of the electron-only device containing P3HT/ PCBA blend film (1:0.7, w/w).

annealing since the P3HT segments looks much more regular with approximate height values around 20 nm. This could be the reason for slightly decreased RMS and increased J_{sc} values, which was consistent with the photovoltaic performance listed in Table 1.

The introduction of a solubilizing group into the phenathrene moiety could improve the solubility of the resulting fullerene derivatives and thus improve the photovoltaic performance of OPVs fabricated using these fullerene adducts as the electron acceptor.

Conclusion

Phenanthrene-substituted fullerene *mono*- (PCMA) and *bis*-adducts (PCBA) were synthesized through a Diels-Alder reaction. The synthesis of the fullerene derivatives was confirmed by ^{1}H NMR spectroscopy and MALDI-TOF mass spectrometry. Both fullerene derivatives showed limited solubility in organic solvents. Organic photovoltaic cells were fabricated using PCBA:P3HT as the active layer. The resultant device has a higher V_{oc} than a device containing $PC_{61}BM$:P3HT fabricated under the same conditions; this is consistent with the higher LUMO energy level of PCBA than that of $PC_{61}BM$. The maximum PCE of the device

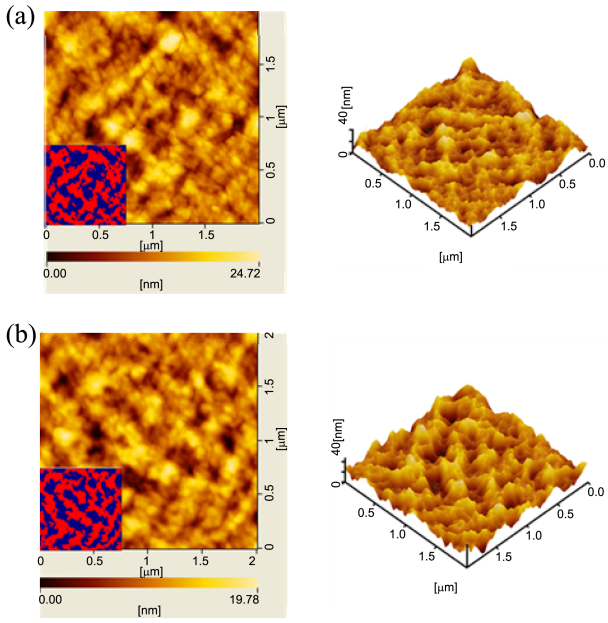

Figure 8. AFM images of P3HT/ PCBA blend films in the pristine state for height, phase (insert), and 3D images (a), and height, phase (insert), and 3D images after thermal annealing at 150 °C for 15 min (b).

fabricated with a PCBA:P3HT active layer is 0.71% using the optimized fabrication conditions.

Acknowledgments. This work was supported by the New and Renewable Energy Program of the Korea Institute of Energy Technology Evaluation and Planning (KETEP) funded by the Korea government Ministry of Trade, industry & Energy (20113010010030), and an NRF grant funded by the Korean government (MSIP) through GCRC-SOP (No. 2011-0030013).

References

1. Armaroli, N.; Balzani, V. *Angew. Chem., Int. Ed.* **2007**, *46*, 52.
2. Pagliaro, M.; Ciriminna, R.; Palmisano, G. *ChemSusChem.* **2008**, *1*, 880.
3. Hauch, J. A.; Schilinsky, P.; Choulis, S. A.; Childers, R.; Biele, M.; Brabec, C. J. *Sol. Energy Mater. Sol. Cells* **2008**, *92*, 727.
4. Lungenschmied, C.; Dennler, G.; Neugebauer, H.; Sariciftci, S. N.; Glatthaar, M.; Meyer, T.; Meyer, A. *Sol. Energy Mater. Sol. Cells* **2007**, *91*, 379.
5. Choi, S.; Potscavage, J. W. J.; Kippelen, B. *J. Appl. Phys.* **2009**, *106*, 054507.
6. Krebs, F. C.; Spanggard, H.; Kjær, T.; Biancardo, M.; Alstrup, J. *Mater. Sci. Eng. B* **2007**, *138*, 106.
7. Bundgaard, E.; Krebs, F. C. *Sol. Energy Mater. Sol. Cell* **2007**, *91*, 1019.
8. Krebs, F. C. *Sol. Energy Mater. Sol. Cells* **2009**, *93*, 1636.
9. Tipnis, R.; Bernkopf, J.; Jia, S.; Krieg, J.; Li, S.; Storch, M.; Laird, D. *Sol. Energy Mater. Sol. Cells* **2009**, *93*, 442.
10. Brabec, C. J.; Padinger, F.; Hummelen, J. C.; Janssen, R. A. J.; Sariciftci, N. S. *Synth. Met.* **1999**, *102*, 861.
11. Brabec, C. J. *Sol. Energy Mater. Sol. Cells* **2004**, *83*, 273.
12. Qian, D.; Ma, W.; Li, Z.; Guo, X.; Zhang, S.; Ye, L.; Ade, H.; Tan, Z.; Hou, J. *J. Am. Chem. Soc.* **2013**, *135*, 8464.
13. Zhou, J.; Zuo, Y.; Wan, X.; Long, G.; Zhang, Q.; Ni, W.; Liu, Y.;

Li, Z.; He, G.; Li, C.; Kan, B.; Li, M.; Chen, Y. *J. Am. Chem. Soc.* **2013**, *135*, 8484.
14. He, Z. C.; Zhong, C.; Huang, X.; Wong, W.-Y.; Wu, H.; Chen, L.; Su, S.; Cao, Y. *Adv. Mater.* **2011**, *23*, 4636.
15. He, Z. C.; Zhong, C.; Su, S.; Xu, M.; Wu, H.; Cao, Y. *Nature Photonics* **2012**, *6*, 591.
16. Mikroyannidis, J. A.; Kabanakis, A. N.; Sharma, S. S.; Sharma, G. D. *Adv. Funct. Mater.* **2011**, *21*, 746.
17. He, Y.; Chen, H.-Y.; Hou, J.; Li, Y. *J. Am. Chem. Soc*. **2010**, *132*, 1377.
18. He, Y.; Zhao, G.; Peng, B.; Li, Y. *Adv. Funct. Mater*. **2010**, *20*, 3383.
19. Meng, X.; Zhang, W.; Tan, Z.; Li, Y.; Ma, Y.; Wang, T.; Jiang, L.; Shu, C.; Wang, C. *Adv. Funct. Mater*. **2012**, *22*, 2187.
20. Ye, G.; Chen, S.; Xiao, Z.; Zuo, Q.; Wei, Q.; Ding, L. *J. Mater. Chem.* **2012**, *22*, 22374.
21. Morinaka, Y.; Nobori, M.; Murata, M.; Wakamiya, A.; Sagawa, T.; Yoshikawa, S.; Murata, Y. *Chem. Commun*. **2013**, 3670.
22. Lenes, M.; Wetzelaer, G.-J.; Kooistra, F; Veenstra, S.; Hummelen, J.; Blom, P. *Adv. Mater*. **2008**, *20*, 2116.
23. Zhao, G.; He, Y.; Li, Y. *J. Am. Chem. Soc.* **2010**, *132*, 1377.
24. Kim, K.-H.; Kang, H.; Nam, S. Y.; Jung, J.; Kim, P. S.; Cho, C.-H.; Lee, C.; Yoon, S. C.; Kim, B. J. *Chem. Mater*. **2011**, *23*, 5090.
25. Mi, D.; Kim, H.-U.; Kim, J.-H.; Xu, F.; Jin, S.-H.; Hwang, D.-H. *Synth. Met.* **2012**, *162*, 483.
26. Mihailetchi, V. D.; van Duren, J. K. J.; Blom, P. W. M.; Hummelen, J. C.; Janssen, R. A. J.; Kroon, J. M.; Rispens, M. T.; Verhees, W. J. H.; Wienk, M. M. *Adv. Funct. Mater*. **2003**, *13*, 43.
27. Hummelen, J. C.; Knight, B. W.; LePeq, F.; Wudl, F.; Yao, J.; Wilkins, C. L. *J. Org. Chem*. **1995**, *60*, 532.